**Supplementary data**

**Facile single step synthesis of flowery shape pure/lithium doped**

**3D iron oxides**

**Rasmita Barik, Brajesh Pandey[#], Shashi Anand, Mamata Mohapatra***

Hydro & Electrometallurgy Department,

CSIR- Institute of Minerals and Materials Technology, BBSR- 751 013, Odisha, India

[ǂ]Deptt. of Applied Science, Symbiosis Institute of Technology, Mulsi, Pune 412 115

* Corresponding author e-mail: mamatamohapatra@yahoo.com

**IR Studies.** The IR spectra of the three samples are shown in Figure $S_3$. In case of sample FeLi-1, the band at 1624 cm$^{-1}$ is assigned to the bending mode of –OH in water. A small broad band at 1386 cm$^{-1}$ confirmed the presence of metal-solvent bonding. It may be due to adsorption of complex solution over iron oxide surface. Appearance of Fe-OH bending mode at 883 cm$^{-1}$ is due to the transition moment lying in the a-b plane; another band at 798 cm$^{-1}$ corresponds to a moment parallel to c axis.[1-2] The absorption bands at 551 and 447 cm$^{-1}$ are assigned to Fe-O stretching and bending vibration mode of $\alpha$-$Fe_2O_3$ respectively. Absorption band near 551 cm$^{-1}$ is assigned to $A_{2u}$ band in hematite matrix [3] and that at 447 cm$^{-1}$ was due to $E_u$ band. The bands at 1624 and 1385 cm$^{-1}$ are significantly reduced in FeLi-2 due to loss of adsorbed water and solvent respectively. Whereas reduction in intensity for 894 and 791 cm$^{-1}$ bands are observed due to phase transformation of ferrihydrite to hematite. The bands related to the Fe-O vibration (551 and 447 cm$^{-1}$ in FeLi-1) became intense and exhibit positive/negative shifts which may be attributed to the smaller particle size, porosity within the body of the nanoparticle, and ion adsorption on the surface. Only two prominent bands at 540 and 466 cm$^{-1}$ were observed for FeLi-3 sample. An increase in the high frequency component at 460 cm$^{-1}$ can be correlated to an increase in the degree of crystallinity.[3] Gradual shifts in the position of characteristic bands of hematite have also been reported due to metal cations substitution.[4]

**X-ray Photoelectron Spectroscopy (XPS) studies.** XPS measurements are carried out to assess the elemental composition and chemical oxidation states of surface and near-surface species. The Fe2p band, composed of the doublet corresponding to Fe2p$_{3/2}$ and Fe2p$_{1/2}$ is of complex character. Besides the main peaks and the Fe2p band envelope from the K$\alpha$ excitation, it contained structures of "shake up" multiplets or shake-up satellite structures. These satellite structures, which are very sensitive to

the electronic structure of the compounds, are frequently used as fingerprints to identify the iron oxide phases. The XPS survey of Fe 2p (Figure $S_4$a) for pure and lithium containing iron oxide samples are shown with the position of the shake-up satellite. Indeed, the binding energy difference between $Fe2p_{3/2}$ and the associated satellite has been reported to be around ~8 eV for Fe(III), while this difference decreases to 4.3-5.6 eV for Fe(II).[5] Therefore, it can be concluded that iron was present exclusively as $Fe^{3+}$ in all the samples. The $Fe2p_{3/2}$ peaks of FeLi-0 occur at 711.6 which correspond to the binding energies of $Fe_2O_3$ and/or FeOOH species [6-7] and the value was slightly lower for annealed samples indicating the phase transition from FeO(OH) to $Fe_2O_3$. This observation is in good accord with the results from the XRD measurements. In addition, $Fe2p_{1/2}$ binding energy is slightly lower in annealed samples. The $O_{1s}$ XPS spectrum of pure hematite showed two components with $O_{1s}$ binding energies at 530.3, and 531.7 eV, assigned to lattice oxygen in hematite and surface defects and/or surface hydroxyls.[8]As for the $O_{1s}$ peak, a slight shift to a higher energy was observed (Figure $S_4$b), The peak shift was attributed to introduction of OH groups due to presence of lithium as hydroxide on surface. On calcination, this peak shifted to lower binding energy showing lithium intercalation in lattice of iron oxide. On further calcination, the peak intensity associated with $O_{1s}$ binding energies at 531.7eV increased along with positive shifting. A slight decrease of binding energy for $Li_{1s}$ (Figure $S_4$c) was observed in FeLi-1 sample as compared to FeLi-0. This decrease implies that the Li atoms were doped into the $Fe^{3+}$ sites to bond with O atoms. However, on further increasing the calcination temperature to 500°C, increase in binding energy of $Li_{1s}$ is observed. It may be due to movement of lithium in to surface defect sites.

1    S. Onari, T. Arai and K. Kudo, *Phys. Rev. B*, 1977, **16**, 1717–1721.

2    C. J. Serna, J. L. Rendon and J. E. Iglesias, *Spectrochim*. Acta, 1982, **38**A, 797–802.

3    I. V. Chernyshova and A. S. Madden, *Chem. Chem. Phys*., 2007, **9**, 1736 −1750.

4    S. Krehula, G. Stefanic, K. Zadro, L. K. Krehula, M. Marcius and S. Music, *J. Alloys Comp.*, 2012, **545**, 200–209.

5    J. M. Cerrato, M. F. Hochella, W. R. Knocke, A. M. Dietrich and T. F. Cromer, *Environ. Sci. Technol*., 2010, **44**, 5881–5886.

6    H. Y. Lin and Y. W. Chen, *Ind. Eng. Chem. Res.*, 2005, **44**, 13, 4569-4576.

7    C. W. Sun, H. Li and L. Q. Chen, *J. Phys. Chem. Solids*, 2007, **68**, 9, 1785-1790.

8    T. F. Moulder, W. F. Stickle, P. E. Sobol and K. D. Bomben Handbook of X-ray photoelectron spectroscopy. Perkin Elmer, Eden Prairie, Minnesota,1992.

**Table S₁** Various solution synthetic routes for development flowery structure $\alpha$-$Fe_2O_3$

| Synthesis Methods | Reagents | Phase | Shape | Application | Ref. |
|---|---|---|---|---|---|
| Solvothermal | $FeCl_3. 6H_2O$ + urea | $\alpha$-$Fe_2O_3$ | porous flowerlike nanosheets, of about 30 nm | semiconductors | [12] |
| Solvothermal | $FeCl_3.6H_2O$ + urea + ethanol tetrahydrofuran (THF), Poly(N-vinyl-2-pyrrolidone) | $\alpha$-$Fe_2O_3$ | oriented-nanocrystals of approximately 20 nm in size | | [13] |
| Hydrothermal | sodium oleate + ethanol + oleic acid + iron (III) chloride hexahydrate aq. solution | $\alpha$-$Fe_2O_3$ | flower-like nanocrystals 30–45 nm in width and 15–25 nm in thickness | | [14] |
| Goethite precursor route | $FeSO_4.7H_2O$ + $CH_3OONa.4H_2O$ | $\alpha$-$Fe_2O_3$ | mesoporous nano structures from hierarchical $\alpha$-FeOOH precursors. | adsorption capacities of 51 and 30 $mgg^{-1}$ for As(V) and Cr(VI) | [15] |
| Solvothermal | $FeCl_3.6H_2O$ + ethanol | $\alpha$-$Fe_2O_3$ | nanorods of dia. 30-40 nm, length: 700-800 nm | Li-Ion Battery, storage device, photocatalytic behaviour | [16] |
| Wet chemical | $FeCl_2.4H_2O$ + CTAB + EG | $\alpha$-$Fe_2O_3$ | surface area is 116 $m^2/g$ average pore size is 7.85 nm. | photocatalysis and lithium ion batteries. | [17] |
| Hydrothermal | Autoclaving of urea + benzene + polyvinylpyrrolidone + containing $Fe(acac)_3$. | $\alpha$-$Fe_2O_3$ | nanobundle-flowerlike microstructures. | photocatalytical and adsorption heavy metal ion Cr(VI). | [18] |
| Precipitation & calcination | $Fe(NO_3)_3$ + $HNO_3$ followed by calcination at 300 $^0$C for 3h | $\alpha$-$Fe_2O_3$ | Flower-like $\alpha$-nanostructures with $\alpha$-FeOOH phase in the | technological applications | [19] |

core

| Method | Precursors / Synthesis | Product | Morphology | Application | Ref |
|---|---|---|---|---|---|
| Hydrothermal | $FeCl_3.6H_2O$ + ($H_2O_2$ 30 wt%) + urea + ascorbic acid ($C_6H_8O_6$) | $\alpha\text{-}Fe_2O_3$ | ---- | environmental remediation | [20] |
| Solvothermal | 70 ml ($FeCl_3 \cdot 6H_2O$), urea, and ethanol) in autoclave kept for 2 min by microwave irradiation and then kept at that temperature for another 30 min under microwave heating. | $\alpha\text{-}Fe_2O_3$ | Flowerlike architectures approximately 0.8−1 μm in diameter. | capacities of 51 and 30 mg $g^{-1}$ for As(V) and Cr(VI) | [21] |
| Solvothermal and calcination | $Fe(NO_3)_3$+ urea + ethylene glycol (170$^o$C) and further calcination at 450$^o$C. | $\alpha\text{-}Fe_2O_3$ | Flowerlike micrometer-sized | - | [22] |

**TableS$_2$** Preparation condition and physico–chemical analysis of synthesized iron oxide samples

| Sample code | preparation condition | %[Fe] | %[Li] | pH | pHpzc |
|---|---|---|---|---|---|
| FeLi-0 | EGME: Fe(III)= 1:6 at 100$^0$C. and 3hr of reaction time | 57.51 | 0 | 1.41 | 6.39 |
| FeLi-0a | FeLi-0 calcined at 400$^o$C | 69.89 | 0 | | 6.86 |
| FeLi-0b | FeLi-0calcined at 500$^o$C | 70.01 | 0 | | 7.21 |
| FeLi-1 | EGME: Fe(III):Li= 1:5:1, LiOH at 100$^0$C and 3hr of reaction time | 63.31 | 2.60 | 1.97 | 4.84 |
| FeLi-2 | FeLi-1calcined at 400$^o$C | 68.11 | 2.65 | | 5.20 |
| FeLi-3 | FeLi-1calcined at 500$^o$C | 68.95 | 2.65 | | 6.06 |

**Table S$_{3(a)}$** XRD data of as prepared and annealed Li doped samples

| Card* | FeLi-0 | FeLi-0(a) | FeLi-0(b) | FeLi-1 | FeLi-2 | FeLi -3 | Plane |
|---|---|---|---|---|---|---|---|
| | 4.31488 | | | | 4.21555 | | |
| 3.7072 | | 3.70742 | 3.62461 | | 3.6986 | 3.59955 | (021) |
| 2.69863 | | 2.69863 | 2.65199 | 2.67603 | 2.72303 | 2.64890 | (104) |
| 2.51428 | 2.50693 | 2.51428 | | | 2.53527 | | (110) |
| | | | 2.46307 | 2.48684 | | 2.48131 | |
| | 2.27025 | | | | | | |
| 2.21005 | | 2.21005 | | | 2.21856 | | (113) |
| | | | 2.17669 | 2.19842 | | 2.17496 | |
| 2.0763 | | 2.07804 | | | | | (022) |
| | 1.99144 | | | | | | |
| 1.84136 | | 1.84136 | 1.82708 | 1.82988 | 1.85193 | 1.82292 | (024) |
| | 1.73658 | | | | 1.70670 | | |
| 1.69882 | | 1.69882 | 1.68482 | 1.68984 | | 1.68216 | (116) |
| 1.60782 | 1.57917 | 1.60782 | 1.57766 | | 1.60723 | 1.58878 | (018) |
| | 1.52425 | | | | | | |
| 1.48655 | 1.47156 | 1.48655 | 1.47985 | 1.47852 | 1.49215 | 1.47777 | (214) |
| 1.45751 | | 1.45751 | 1.44250 | 1.44508 | 1.46007 | 1.4429 | (300) |

*d* values

RRelative intensities (% RI)

| Card* | FeLi-0 | FeLi-O(a) | FeLi-O(b) | FeLi-1 | FeLi-2 | FeLi -3 | Plane |
|---|---|---|---|---|---|---|---|
| 25 | 27.29 | 32.58 | 21.23 | 86.44 | 11.16 | 19.26 | (021) |
| 100 | 100.00 | 100.00 | 100.00 | 100.00 | 100.00 | 100.00 | (104) |
| 50 | 44.22 | 82.41 | 81.28 | 52.08 | 80.36 | 95.11 | (110) |
| 30 | 7.80 | 30.76 | 34.99 | 16.81 | 33.89 | 36.17 | (113) |
| 40 | 43.47 | 51.13 | 51.66 | 39.48 | 24.49 | 58.12 | (024) |
| 60 | 40.67 | 72.45 | 85.71 | 96.96 | 49.46 | 76.93 | (116) |
| 35 | 54.71 | 49.94 | 60.82 | 26.02 | 9.31 | 18.80 | (018) |
| 35 | 41.80 | 50.84 | 68.47 | 60.47 | 34.94 | 62.82 | (214) |
| 20 | 8.00 | 19.48 | 17.56 | 98.64 | 37.08 | 67.18 | (300) |

**Table S$_{3(b)}$** Lattice parameters, unit cell volume, average grain size of Synthesized samples.

| Crystals | Lattice parameters | | | Unit cell volume | Average grain Size, nm |
|---|---|---|---|---|---|
| | a | b | c | | |
| FeLi-0 | 3.27 | 9.79 | 4.30 | | |
| FeLi-0(a) | 4.56 | 4.56 | 12.78 | | |
| FeLi-0(b) | 4.45 | 4.45 | 12.56 | | |
| FeLi-1 | 4.35 | 4.35 | 12.21 | 200.14 | 18.8 |
| FeLi-2 | 4.32 | 4.32 | 12.10 | 195.62 | 23.5 |
| FeLi-3 | 4.32 | 4.32 | 12.06 | 193.11 | 22.9 |

**Table S$_4$** Mössbauer parameters. Uncertainty in isomer shift ($\delta$); Quadrupole splitting ($\Delta$) and Line width ($\Gamma$) is 0.02 mm/s while that in hyperfine field (B) is 0.5 T; Areas are accurate within $\pm 2\%$.

| | IS ($\delta$) mm/s | QS ($\Delta$) mm/s | LW ($\Gamma$) mm/s | B$_{HF}$ (T) | Area (%) | Iron Phases |
|---|---|---|---|---|---|---|
| FeLi-0 | -0.01 | - | 0.28 | | 10.5 | Goethite |
| | 0.35 | 0.52 | 0.46 | | 89.5 | Ferrihydrite |
| FeLi-1 | 0.32 | 0.59 | 0.54 | | 52 | Ferrihydrite |
| | 0.34 | -0.18 | 1.00 | 46.8 | 48 | Hematite |
| FeLi-2 | 0.20 | 0.32 | 0.31 | | 8 | Goethite |
| | 0.35 | -0.21 | 0.27 | 51.4 | 92 | Hematite |
| FeLi-3 | 0.36 | -0.21 | 0.33 | 51.3 | 100 | Hematite |

**Table S$_5$** Langmuir and Freundlich parameters for adsorption of fluoride on iron oxide samples

| Sample Langmuir coefficients | | | | Freundlich coefficients | | |
|---|---|---|---|---|---|---|
| Name | $q_m$ (mg g$^{-1}$) | b (L g$^{-1}$) | $R^2$ | $K_F$ | n | $R^2$ |
| FeLi-1 | 151.5 | 0.10 | 0.95 | 1.11 | 2.0 | 0.99 |
| FeLi-2 | 111.1 | 0.20 | 0.97 | 1.0 | 1.9 | 0.99 |
| FeLi-3 | 113.63 | 0.08 | 0.94 | 0.97 | 1.50 | 0.986 |
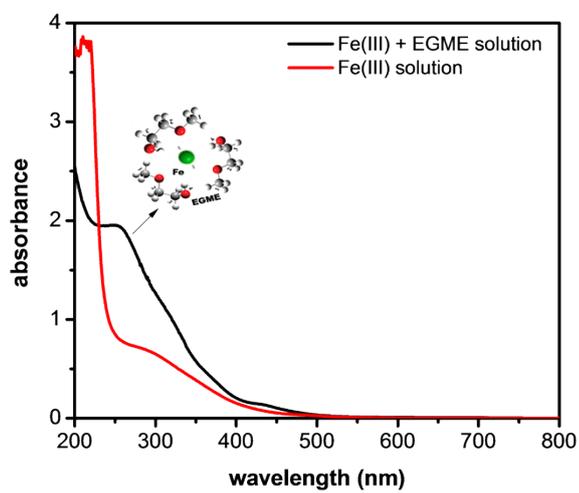
**Figure S₁** Uv-vis spectra of iron solution with and without EGME.
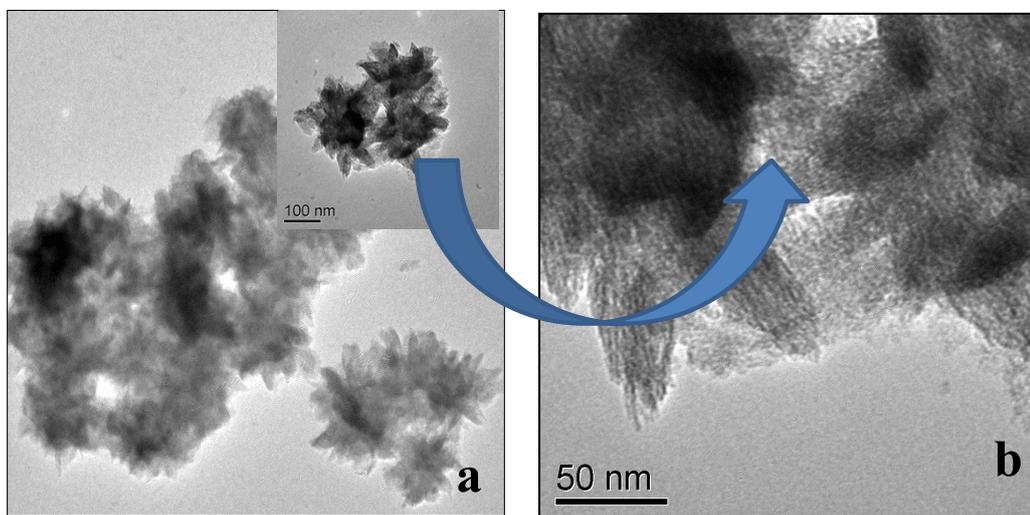
**Figure S₂** (a) TEM image of FeLi-0 (b) Magnified TEM image. The average particle size of 2-5 nm are calculated during TEM measurement at different spot of Figure S₂b.
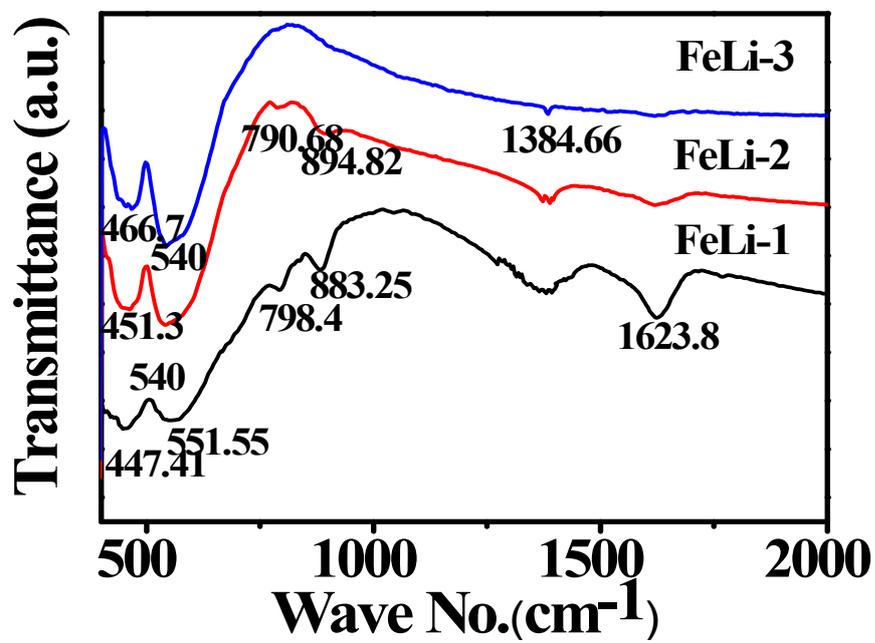
**Figure S$_3$** FTIR spectra of iron oxide samples.
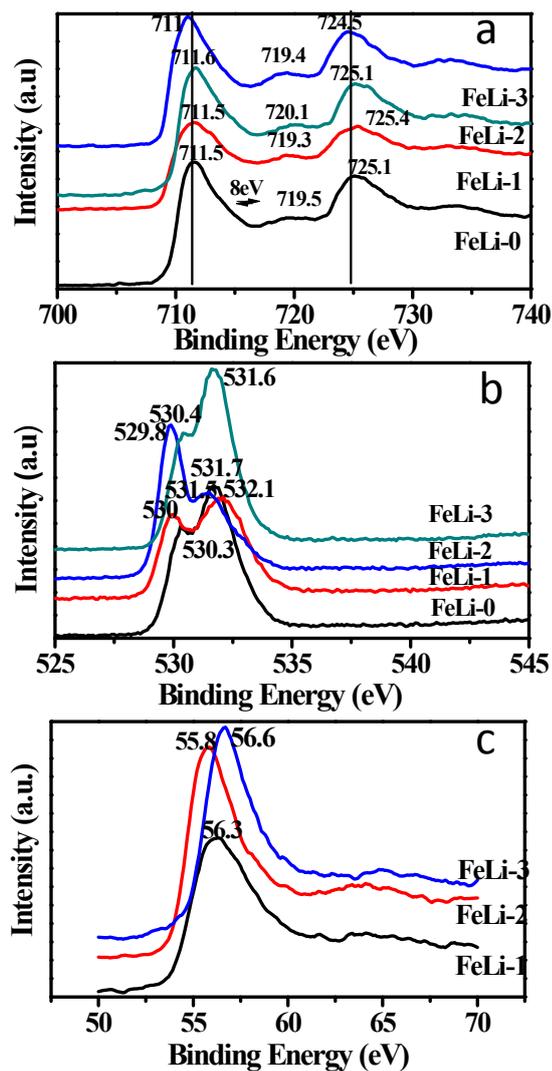
**Figure S₄** XPS spectra (a) Comparing Fe2p spectra of as synthesized and annealed lithiated iron oxide samples. Difference between Fe2p$_{3/2}$ and the associated satellite has shown around ~8 eV indicating +3 oxidation state of iron. (b) O$_{1s}$peaks located between 531.5–532.1 eV attributed to OH species and peaks, at around ~530 eV corresponding to O-Fe bonds. (c) binding energy for Li$_{1s}$
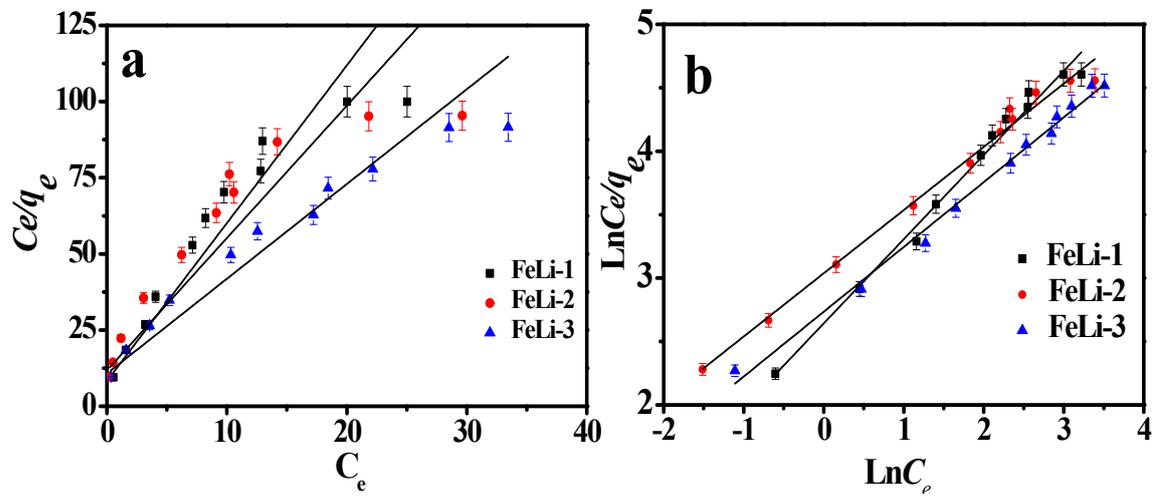
**Figure S$_5$** (a) Langmuir and (b) Freundlich plots